Characterization of deep levels introduced by alpha radiation in *n*-type silicon

M. Asghar, M. Zafar Iqbal, and N. Zafar
Semiconductor Physics Laboratory, Department of Physics, Quaid-i-Azam University, Islamabad, Pakistan

(Received 14 September 1992; accepted for publication 17 December 1992)

A detailed deep-level transient spectroscopy study of the characteristics of deep-level defects introduced by 5.48 MeV alpha particles in low-doped *n*-Si is reported. The deep-level characteristics studied include emission rate signatures, activation energies, capture cross sections and their temperature dependence, and defect concentrations and their spatial profiles. At least five deep levels in the upper-half band gap and two levels in the lower-half gap have been observed as a result of irradiation and characterized in detail. A systematic study of their generation rates up to a dose of about 3×10^{10} alpha particles/cm^2 has been performed providing insights into the dose dependence of their formation mechanisms. Interesting room temperature transformation phenomena have been observed in our deep-level spectra during room temperature storage of the irradiated samples. Extensive isochronal thermal annealing measurements have been carried out to obtain data on the anneal-out characteristics of the radiation-induced deep levels and to identify these with the known defects wherever possible. A number of new annealed-in levels have been observed during this investigation. A detailed comparison with the published results is presented.

I. INTRODUCTION

The study of radiation damage in solids has been an important theme of research of interest to fundamental physics of solid state as well as to the applications of solid materials.[1] In semiconductors such studies assume paramount importance in view of the extreme sensitivity of their electronic characteristics to the defects produced by interaction with radiation. The obvious examples of this aspect are the degradation of photovoltaic solar cells in prolonged use in upper space and the semiconductor electronic devices in nuclear reactor environments. On the other hand the study of radiation-induced crystal defects in semiconductors yields a wealth of information which has been extremely useful in understanding the nature of defects and their formation mechanisms[2] and in revealing new phenomena in semiconductors.[3] The investigation of radiation-induced defects, therefore, continues to be a subject of considerable interest in semiconductor research.

Although most of such studies have been carried out using high energy electron radiation to simulate closely the cosmic radiation effects on silicon solar cells in space, some reports exist on the defects induced by other radiation such as γ rays,[4] protons,[5] laser radiation[6] and neutrons,[7] while studies reporting interaction of α radiation with silicon are few.[8–12] The use of α particles for such studies while being of inherent interest in view of their large mass and charge is highly motivated by the recent realization that α particles emitted from packaging materials are a major source of soft[13] and hard[14] errors in dynamic random-access-memories (DRAM) and charge-coupled devices (CCD). The understanding of the nature and role of α radiation induced defects in Si is, therefore, extremely important to the further progress of the very large scale integrated (VLSI) device technology. The present study is clearly of great current interest and potential benefit against this perspective.

The few previously available studies of alpha irradiation of silicon have been carried out on *n*-type material employing either p^+n junctions or Schottky barriers, often containing significant concentrations of inadvertent residual defects before irradiation. The presence of these inadvertent defects naturally enhances the possibility of formation of unknown complexes with radiation-induced defects and leads to erroneous interpretations of results. The background doping concentrations of shallow impurities also need to be low for the same reason and also to enhance the detection sensitivity for the deep-level defects produced by irradiation. Our study has been carried out on low doped *n*-type silicon samples with very low inadvertent deep-level content. Thus our study enabled us to investigate the radiation-induced deep-level defects spanning the entire band gap of silicon with high sensitivity and without any interference from the inadvertent levels. Detailed characterization of carrier emission rates, capture cross sections, and concentration profiles of defects has been carried out using deep-level transient spectroscopy (DLTS) technique.[15] Peak shape analysis has been performed on each DLTS peak for a better understanding of the deep-level characteristics. In addition, detailed production rate and annealing studies have been carried out to obtain a comprehensive picture of the α radiation induced defects in *n* silicon.

II. MATERIAL AND EXPERIMENTAL DETAILS

Our *n*-type silicon samples consisted of prefabricated p^+n junction diodes having an area ~1.5 mm^2 prepared on low-doped *n*-type epitaxial material. The *n*-type region comprised 10–20-μm-thick epitaxial layers on n^+ substrates of Czochralski silicon. The doping concentrations

 0021-8979/93/083698-11$06.00

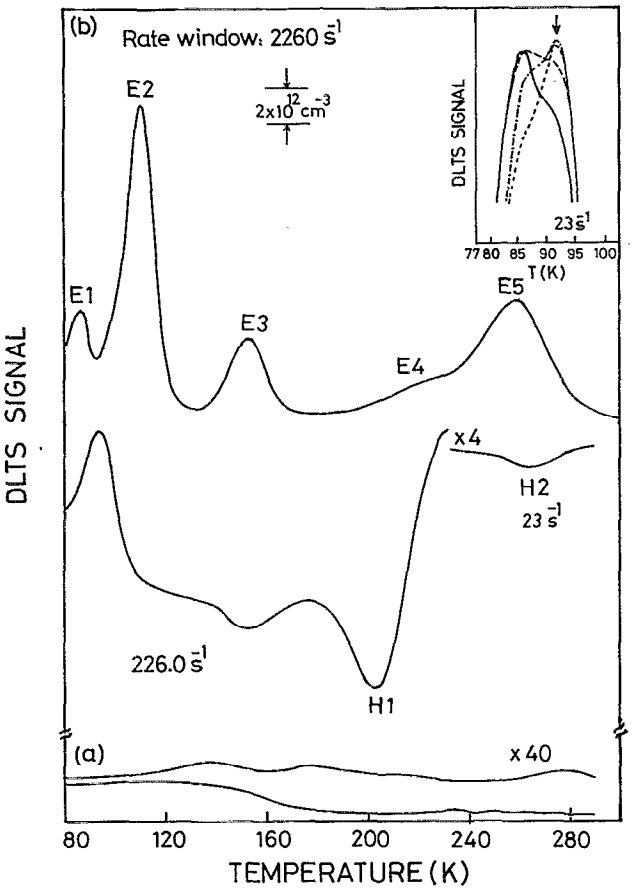

FIG. 1. DLTS spectra of (a) unirradiated p^+n junction diodes, (b) α-irradiated samples exposed to a dose of 3.2×10^{10} cm^{-2} (of 5.48 MeV α particles). The inset shows details of metastable spectral features observed in the vicinity of peak E2 during different DLTS scans—arrow indicates the usual position of the peak E2 at this rate window setting. Excitation pulse: -3.0 V to -0.5 V for majority-carrier DLTS (upper curves in a and b) and 0 V to $+1$ V for injection DLTS (lower curves).

on the n side of the junction, as obtained from capacitance-voltage (C-V) measurements, were typically 2–4×10^{14} cm^{-3}. Ohmic contacts were provided to the n-type back side by using Ga-Al amalgam while the front contact was provided by ultrasonic bonding to a TO-5 header lead. The typical DLTS spectra of the unirradiated p^+n junctions for majority- and minority-carrier emission are given in Fig. 1(a). The spectra are extremely clean showing insignificant background deep-level concentrations typically of the order of $\sim5\times10^{10}$ cm^{-3}.

DLTS measurements were performed using a Metrimpex (Hungary) deep-level spectrometer Model DLS-81, based on the lock-in principle. The details of the instrument are described in Ref. 16. The samples on TO-5 headers were mounted in a variable-temperature cryostat with a symmetrically placed TO-5 header to which was attached a copper-constantan thermocouple to monitor the sample temperature. The sample temperature could be varied from 77 K, by lowering the carefully shielded metallic block holding the sample and the thermocouple into a liquid nitrogen dewar, to higher than room temperature by using a heater embedded in the metallic block. An automatic motor-driven variable capacitor was used to compensate for the background standing capacitance of the sample.

After routine assessment including current-voltage, capacitance-voltage and DLTS measurements the selected samples were exposed to α radiation from an ^{241}Am source emitting 5.48 MeV α rays at room temperature. First DLTS measurements were always performed with a minimum loss of time (approximately 10–15 min) after terminating irradiation to minimize any loss of information due to room temperature annealing effects.

III. MEASUREMENTS

Our experimental investigations consisted of the following measurements on each DLTS peak observed in our irradiated samples.

A. Emission rates

Data were obtained over as wide a range of temperatures as possible and an Arrhenius plot analysis was used to obtain the activation energy (from the slope) and the infinite-temperature capture cross section (from the intercept) of the various observed deep levels.

B. Concentration profiles

Differential DLTS feature of our spectrometer was used to obtain precise depth profiles of the concentrations of various deep levels normal to the junction plane. In this mode of operation, our instrument measured a DLTS signal corresponding to the difference of the capacitance transients arising due to two excitation pulses with a preset height difference applied in sequence. Care was taken to measure the DLTS signal from as small a slice of the device as possible to obtain an accurate concentration profile. The data always showed a sharp decline close to the edge of the depletion region which is superficially introduced by the well-known edge region effects of the free-carrier tails. Accordingly the data were discarded beyond boundary of the edge region obtained from Eq. (3.12) of Ref. 17.

C. Capture cross sections and their temperature dependence

Direct measurements of the capture cross sections were carried out using the usual variable-width single pulse method as well as a double pulse method. In the latter method the first wide pulse is used to fill the deep levels to saturation followed by a second pulse whose width is varied from scan to scan, while DLTS is operated in the differential mode to obtain better accuracy for peak height measurement at low capture times. Since the long capture-pulse measurements are strongly influenced by the presence of nonexponential behavior of the transients due to additional deep levels as well as the edge-region-capture effects, this method is expected to provide more accurate values of the capture cross sections.

Capture cross sections for the majority carriers were measured both for the electron- and hole-emitting levels

(i.e., the majority and minority carrier peaks) in a given sample. In the case of minority-carrier peaks the levels were filled with minority carriers using strong injection pulses followed by a majority carrier (reduced reverse bias) "clear" pulse of varying duration from scan to scan, as suggested by Lang.[17] The reduction rate of the minority-carrier peak height would clearly yield the majority-carrier capture cross section.

The data were analyzed using a semilogarithmic plot of the peak height reduction $[1-S(t_p)/S(\infty)]$ with respect to the saturated peak height $S(\infty)$ versus the variable pulse width t_p in the usual way. Whereas the data for a single deep level transient should theoretically fit a single exponential decay on such a plot, in practice it never happens due to nonexponentialities introduced by the contributions of the carrier tails (edge effect) and the other nearby levels, if any, giving overlapping peaks. Our data for the various radiation-induced defects are found to be highly nonexponential. We have, as a rule, tried to correct our data for the edge region effects following Meijer *et al.*[18] This consists in plotting the data obtained from our capture measurements on a $[1-S(t_p)/S(\infty)]$ vs $\log(t_p)$ graph—the long-time part of this curve is expected to be linear if caused by the edge effect. The data points are then corrected by subtracting the edge region contribution obtained by extrapolating this linear part back to $t_p=0$ from the measured values. The corrected data are then plotted as a $[1-S(t_p)/S(\infty)]$ vs t_p graph and the values of capture rates $[c=\sigma v_{\rm th}(T)n]$ at the temperature of measurement T are obtained from the slope(s) of the exponential part(s)of the plot. The corresponding capture cross sections are thereby calculated by using the free carrier concentration n determined from C-V analysis and the thermal velocity $v_{\rm th}$ of the carriers at the appropriate temperature. The effective mass values for electrons and holes in silicon[19] used for the respective velocities are $m_e^*=1.1m_e$ and $m_h^*=0.52m_e$, where m_e is the free electron mass. To investigate the temperature dependence of the capture cross sections, these experiments are repeated for different DLTS emission rate windows.

D. Peak-shape profiles

To investigate the detailed structure of our DLTS peaks and to gain further insight into the results of our capture cross-section measurements, we analyzed the shape profiles of the observed peaks against the theoretically predicted DLTS peak profiles to be expected on the basis of our emission data for the respective peaks. The DLTS peak-profile formula given by Lang[17]

$$A(y)=\frac{2\pi(1-e^{-y})}{4\pi^2+y^2},$$

(where $y=T/\tau$, T being the reciprocal of the lock-in frequency and τ the transient time constant), was used to fit our observed peak shapes, thereby providing evidence as to whether our peaks were associated with clearly resolved deep levels or produced by emission from multiple deep levels having close energy and/or emission rate signatures. In the latter case of a structured peak we have tried to extract as much information on the characteristics of the additional overlapping peaks as possible by subtracting out the contribution of the main peak from DLTS spectra obtained for a number of rate windows, subjecting each such spectrum to the peak-shape analysis for all the peaks.

The peak-shape fitting procedure had been previously tested on some of the isolated DLTS peaks known to be produced by single deep levels in some of our earlier works.

IV. RESULTS

A. Deep level spectra

The DLTS spectra for majority-carrier emission and minority-carrier emission from deep levels after alpha irradiation of our p^+n diodes are shown in Fig. 1(b). The spectra, as presented in a preliminary communication,[20] show at least five electron emission peaks named E1 to E5 and two hole emission peaks named H1 and H2, in addition to a broad band of hole levels at the low temperature end of the injection spectrum. The low temperature electron emission peak in this spectrum shows a certain metastability effect insofar as we observe a compound peak structure in this temperature region in identically repeated DLTS scans. This feature is displayed in the inset of Fig. 1(b). Our detailed investigation of this feature using various combinations of the DLTS measurement parameters such as emission rate window, capture pulse width, reverse bias, time and temperature of application of the bias and the pulse, and previous history of the DLTS scans has not led to a definitive identification of the experimental parameters required to reproducibly see this metastability effect. It is most probably some peculiar, maybe critical, combination of these experimental parameters that leads to this effect. Although we cannot make an unequivocal identification of its origin, it is likely that this effect is similar in origin to the effect observed by Jellison[21] on electron-irradiated silicon.

B. Emission rate signatures and activation energies

The emission rate signatures of the observed defect centers were measured over as wide a range of temperatures as possible and are presented in Fig. 2 as the usual T^2-corrected Arrhenius plots. The activation energies and the capture cross sections at infinite temperature obtained from the slopes and intercepts of these plots are given in Table I. No detailed measurements could be performed on the hole emission band observed in our injection DLTS spectrum. However, we can estimate the position of the top of this band of deep levels from the temperature position of the band to be approximately $E_v+0.35$ eV.

C. Capture cross sections

The results of the capture cross-section measurements are outlined below for various levels.

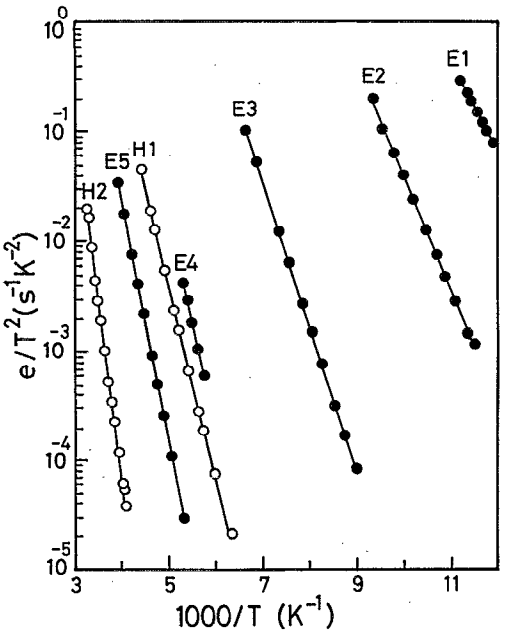

FIG. 2. Emission rate signatures of the α-induced deep levels in n-silicon.

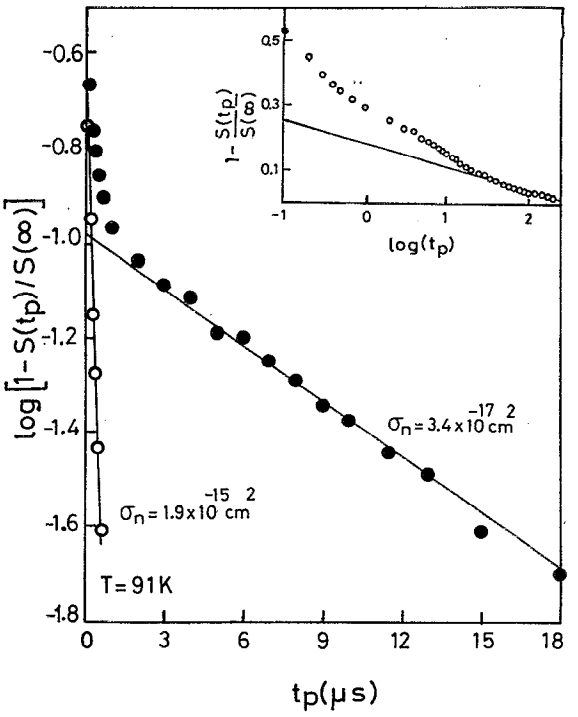

FIG. 3. Capture cross section of the electron level E2: DLTS peak height S measured as a function of the excitation pulse width t_p at 91 K. The inset shows the edge region contribution. The data points after subtracting this contribution are plotted in the main graph.

1. E1

The capture cross section of this level was not measured since it appeared as a small shoulder on the much bigger peak corresponding to the level E2.

TABLE I. Measured characteristics of α particle induced deep level defects in silicon. $\sigma(\infty)$: thermal capture cross sections for electron (n) or hole (p) obtained from the emission rate data. $\sigma(T)$: electron capture cross sections directly measured at temperature T. N_T: typical measured deep-level concentration. η: production rate.

Peak name	Level position (eV)	$\sigma(\infty)$ ($\times10^{-13}$) (cm^2)	$\sigma_n(T)$ ($\times10^{-16}$) (cm^{-3})	N_T ($\times10^{12}$) (cm^{-3})	η (cm^{-1})	T_{out} (°C)
E1	$E_c-0.166$	2.3(n)	⋯	6.5	>61[a]	135
E2	$E_c-0.204$	2.2(n)	0.34 19.00 (91 K)	18.2	>420[a]	400
E3	$E_c-0.261$	0.17(n)	>2.10 0.18 0.82 (133 K)	4.0	134.3	275
E4	$E_c-0.370$	0.14(n)	⋯	2.0	60.9	100
E5	$E_c-0.430$	0.03(n)	0.32 7.70 (206 K)	5.0	160.2	275
E6	$E_c-0.315$	0.11(n)	0.35 8.70 (160 K)	4.0	⋯	⋯
H1	$E_v+0.352$	0.03(p)	>0.13 0.03 (215 K)	>13.0	>414	>400
H2	$E_v+0.652$	10.0(n)	8×10^{-4} 0.17 (279 K)	>0.5	>10	135

[a]These lower limits have been obtained from the linear parts of the curves for E1 and E2 in Fig. 7.

2. E2

The peak height reduction data for this level are plotted in Fig. 3 on a log-linear plot. The data clearly show highly nonexponential decay of DLTS peak height $[1-S(t_p)/S(\infty)]$ with pulse width t_p. The data were corrected for the depletion region edge effect as shown in the inset using the procedure elaborated in Sec. III C and the corrected data were found to fit a sum of two exponentials. This indicates that two different deep-level states are probably contributing to this apparently single peak. The initial part of the data was consequently corrected by subtracting the contribution of the second exponential and the electron capture cross sections obtained for the two states presumed to contribute to this peak. The values of these capture cross sections are given in Table I. These cross sections were measured over the temperature range 83–95 K but no significant variation was found.

3. E3

The capture cross section data for this level turned out to be most complex. The data are plotted in Fig. 4. Even after the edge region correction, the data seemed to correspond to a sum of more than two exponentials. The initial part of the data (up to $t_p=1$ μs) showed an oversubtraction after the edge region correction, which is understandable in view of the different time scales of the capture processes of the more-than-two states involved in these measurements on the E3 level. For the initial part, therefore, we could only obtain a lower limit for the capture cross section from the original (uncorrected for edge

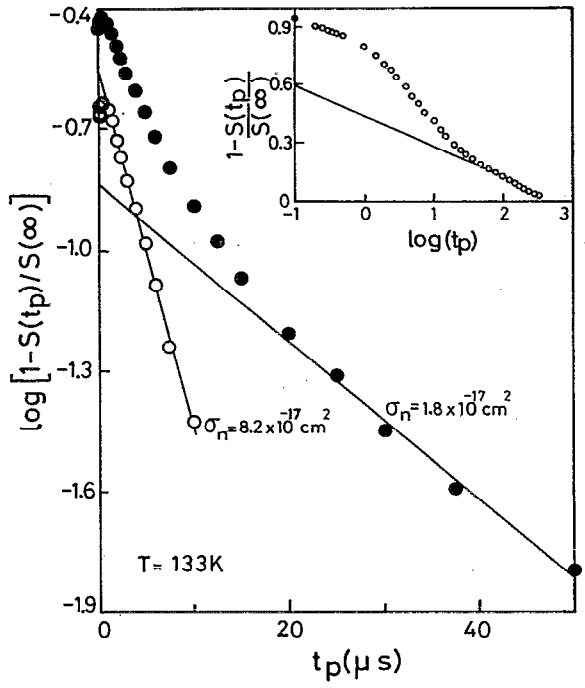

FIG. 4. Capture cross-section data for the electron level E3 at 133 K. The inset shows the edge region contribution which is subtracted out in the main graph. The data in the initial part of the curve (up to ~ 1 μs) are oversubtracted after edge region correction. The capture cross section for this part is estimated from the uncorrected data.

region) data. Three capture cross sections are thus obtained from measurements on this peak corresponding to the initial, middle, and long time part of the capture data shown in Fig. 4. These values, given in Table I, may correspond either to three deep-level states contributing to the same main peak E3 or to the overlapping peaks on the low and high temperature sides of this peak as revealed by our peak-shape analysis to be discussed later. The capture cross-section measurements on this peak were carried out over the temperature range 116–133 K and again no significant temperature dependence was observed for these capture cross sections.

4. E4

No capture cross-section measurements could be carried out on this peak since it has a strong overlap with the bigger peak E5.

5. E5

The usual analysis showed the data to fit a sum of two exponentials, yielding two values for the electron capture cross sections corresponding, presumably, to two states contributing to these measurements. No significant temperature dependence of these electron capture cross sections was detected from measurements over the temperature range 195–218 K. The values of the capture cross sections for this peak are given in Table I.

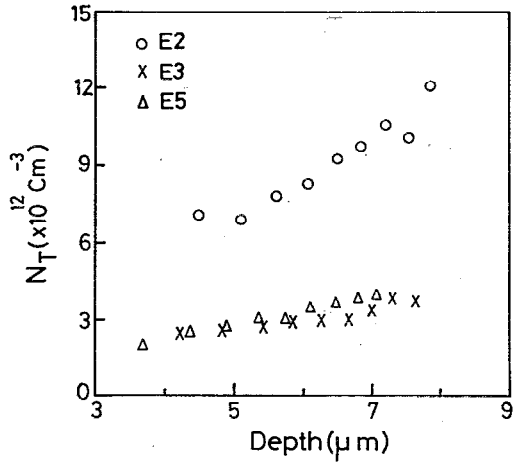

FIG. 5. Spatial profiles of the defect concentration in p^+n diodes due to α-particle irradiation. The depth below the metallurgical junction on the n side is plotted on the horizontal axis.

6. H1

Although this peak corresponds to minority-carrier (hole) emission, the electron capture cross section of this level could be measured in the p^+n samples as explained in Sec. III C. No meaningful analysis with edge-region correction could be performed on the data since such a procedure resulted in a very significant oversubtraction of the initial part similar to the case of the E3 level. The straightforward analysis without edge region correction showed that most of the data could be fit to a sum of two exponentials. The values of the electron capture cross sections so obtained are given in Table I.

D. Concentration profiles

The concentration profiles of the deep levels which could be conveniently measured are shown in Fig. 5. The concentration of the most prominent level E2 is clearly seen to increase gradually from metallurgical junction to the bulk region. The distribution of the radiation-induced defects corresponding to the levels E3 and E5 is found to be almost uniform throughout the space charge region of the junction as shown in Fig. 5. It is interesting to note that these two deep levels have almost identical concentrations and distribution profiles indicating that these levels probably originate from the same defect, a point that will be discussed in detail later on.

E. DLTS peak-shape analysis

The peak-shape analysis on DLTS spectra obtained immediately after irradiation clearly showed that none of the observed electron peaks corresponded to a single deep level but was a result of more than one overlapping peaks. The detailed analysis of the components of each peak, using the procedure outlined in Sec. III D for spectra obtained for four different emission rate windows, was carried out on irradiated samples in which the peak E4 had already ceased to be clearly visible and the peak E6, to be

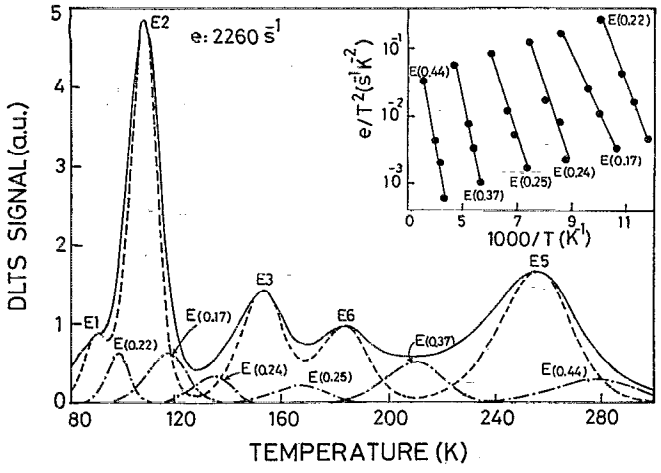

FIG. 6. DLTS peak shape analysis of the radiation induced electron emission peaks: excitation pulse: -3.0 V to -0.5 V, width: 50 μs. Solid curve: observed spectrum, dashed curve: theoretical spectrum obtained from line fit for dominant peaks, dot-dashed curve: residual peaks resulting from a comparison of the two. The inset shows the estimated emission rate signatures of the additional electron levels obtained by the peak shape analysis of spectra at four different rate windows.

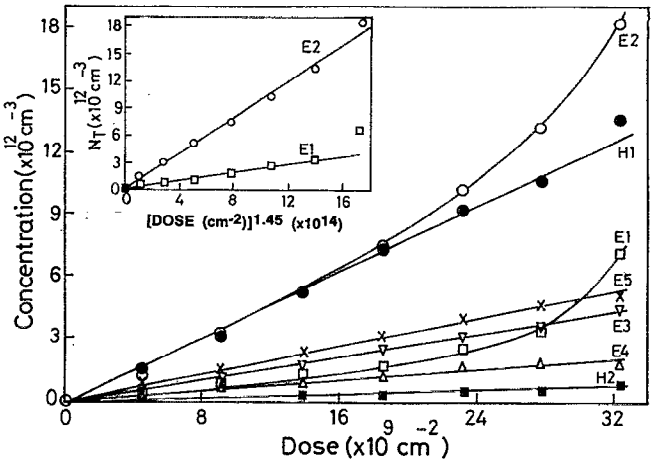

FIG. 7. Dependence of concentrations of radiation-induced defects on alpha-particle dose. The inset indicates the $\phi^{1.45}$ power law fit for the dose (ϕ) dependence of the production data of E1 and E2 levels.

discussed in Sec. IV G, had been generated during room temperature storage. The results of such an analysis are presented in Fig. 6. At least six new peaks are found to be hidden in our majority-carrier spectra in addition to the prominent peaks that are clearly visible in the experimental DLTS scan. Their approximate energy levels and emission rate signatures extracted from our peak-shape analysis are given in the inset of Fig. 6. In the light of this analysis it is clearly understandable as to why our capture cross-section data are so complex for every radiation-induced peak as described in Sec. IV C.

F. Production rates

The dose dependence of the generation rate of the various deep levels was studied from a dose of $\sim 4\times 10^{9}$ cm^{-2} up to $\sim 3.2\times 10^{10}$ cm^{-2}. The results are shown in Fig. 7. The concentration of the deep levels produced increases almost linearly with dose for most of the levels. Both E1 and E2 show a trend towards supralinear increase in generation rate. A power-law analysis of these production rate data led us to a ϕ^{n} dependence with $n=1.45$ for both the levels at least up to a radiation dose $\phi=2.8\times 10^{10}$ cm^{-2}, as shown in the inset of Fig. 7.

The concentrations of the hole levels H1 and H2 should only be considered as a lower limit because of the expected incomplete filling of the minority-carrier levels during injection DLTS experiment. It is clear from our data that the production rates of the deep levels observed in our study increase in the following order: H2, E4, E1, E3, E5, H1, and E2.

The actual production rates as obtained from the slopes of linear fits to these data are given in Table I and are seen to cover the range $\sim$60–400 cm^{-1} for the electron levels while the lower limits for the hole levels H1 and H2 are $\sim$400 cm^{-1} and $\sim$10 cm^{-1}, respectively.

G. Annealing characteristics

1. Room temperature annealing

During storage at room temperature, interesting transformations were observed in the DLTS spectra of our samples. In Fig. 8 are shown the electron emission spectra on the same sample taken immediately after irradiation and

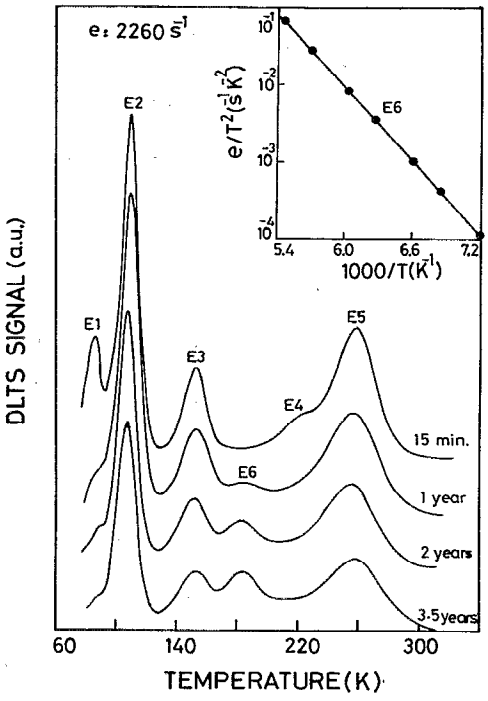

FIG. 8. DLTS spectra of a sample as a function of the storage time at room temperature. Note the E6 peak emerges and increases with time. The inset shows the measured emission rate signature of the E6 level.

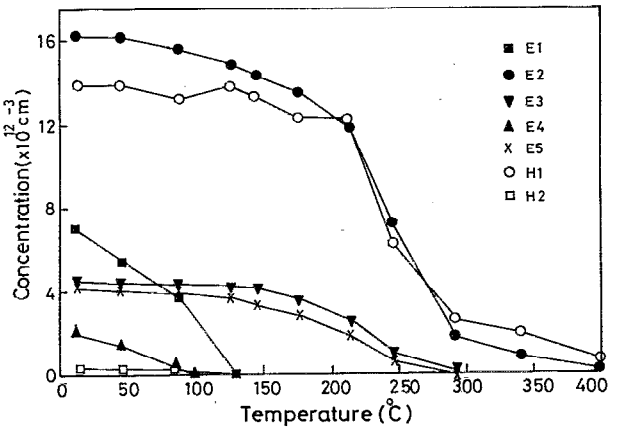

FIG. 9. Isochronal annealing characteristics of α-radiation-induced deep levels in n-silicon. Anneal time at each temperature: 20 min.

those taken after long storage times following irradiation. The following important effects can be clearly inferred from a comparison of these spectra:

(i) The pronounced shoulder corresponding to the deep level E4 is seen to disappear with storage.

(ii) A new electron emission peak labeled E6 is clearly seen to emerge and increase with storage time as a result of room temperature annealing. The emission rate data on level E6, plotted in the inset of Fig. 8, yields the energy position of this level to be $E_c-0.315$ eV.

(iii) An overall decrease in all the other peaks can be noticed with long storage times. This has obvious implications for the long term use of the radiation-induced-defect control of electronic characteristics of silicon devices.

2. High temperature annealing

The annealing study was undertaken to shed light on the defect structure of the deep levels and to help identify the origin of these defect centers. Isochronal annealing was performed for 20 min in steps of 20–30 °C in nitrogen ambient, each followed by a DLTS measurement. The concentration data obtained for the various deep levels from these experiments are plotted in Fig. 9 as a function of the annealing temperature up to 400 °C.

The level E4 is the first to disappear at ~100 °C. Next to disappear is the deep level defect E1 which anneals out at about 135 °C. Levels E3 and E5 remain more or less undiminished up to about 150 °C and then drop in concentration progressively, finally disappearing together at ~300 °C. While the exact temperature at which they completely anneal out varies somewhat from sample to sample (being as high as ~350 °C in other samples), the coincidence of this temperature for these two levels is a recurring feature. The deep-level E2 tends to decrease gradually beyond ~50 °C diminishing monotonically to almost zero concentration at 400 °C. Although the exact annealing characteristics of the hole (minority-carrier) level H1 are difficult to obtain accurately because of the possible changes in the injection characteristics of our samples due

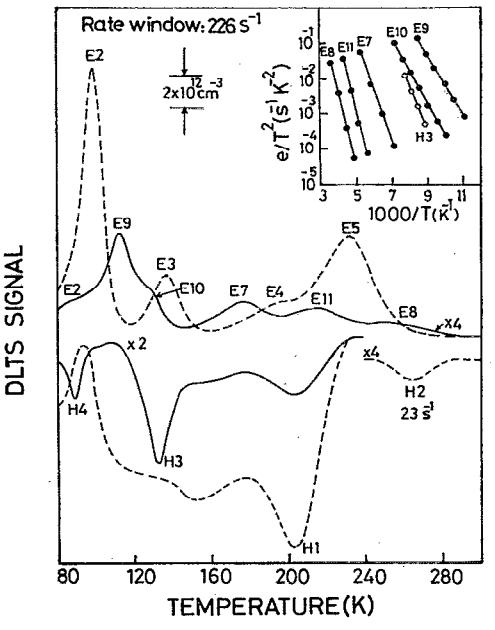

FIG. 10. Typical DLTS spectra of a diode irradiated with 3.2×10^{10} cm^{-2} α-particle dose. Dashed: as irradiated; solid: after the 340 °C annealing step. All the annealed-in deep-level peaks can be seen in this spectrum.

to heat treatment, we generally find H1 to follow E2 in its annealing characteristics. The hole level H2 anneals out at about 135 °C almost concurrently with E1.

3. Annealed-in levels

At least five new electron levels appear to be generated while two new hole levels are annealed in during high temperature treatment of our irradiated samples. Typical majority-carrier and injection DLTS scans taken at the termination of the 340 °C annealing stage and the Arrhenius plots of the annealed-in levels (inset) are shown in Fig. 10. Two minority carrier peaks H3 and H4 are seen to emerge in the region where a broad band was observed in the spectrum immediately after irradiation (Fig. 10). The apparent peak H4 is probably only a part of a new minority-carrier peak which strongly overlaps the adjoining strong peak E9, since it shows an erratic shift with the emission rate window and hence no reliable emission rate data and activation energy could be obtained for this level. The annealing curves of these new levels are presented in Fig. 11. The detailed electrical characteristics of these levels are listed in Table II.

V. DISCUSSION

A number of deep levels have been observed as a result of alpha-particle irradiation of p^+n Si junctions in our study. Some of these levels can be identified with the radiation induced defects known from previous studies using other types of radiation (notably electrons), while others appear to be observed for the first time in our study. A detailed comparison with literature and discussion of each deep level follows.

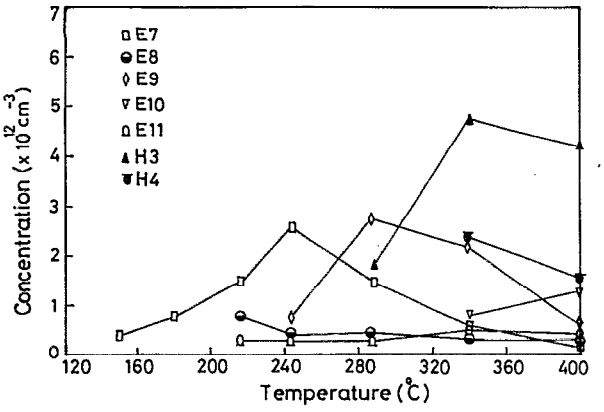

FIG. 11. Isochronal annealing characteristics of the annealed-in deep levels in irradiated n-silicon.

A. E1 - electron level at $E_c-0.166$ eV

This level was at first thought to be caused by the well-known A center since its activation energy is close to that of the A center commonly observed in the irradiation work on silicon. However, our isochronal annealing study clearly showed that it cannot be the A center since this level is found to disappear at about 135 °C (Fig. 9) whereas most of the reported work[22–24] shows the A center to anneal out at temperatures ranging from 300 °C to 400 °C. The production rate of this level has a nonlinear dependence on the radiation dose, increasing supralinearly. The nonlinear dose dependence and the similarity of the activation energy suggest that this level is probably the 0.15 eV level observed by Gubskaya *et al.*[9] in their alpha-irradiation work. They have not reported any annealing characteristics of this level. We find this level to be relatively unstable to thermal treatment, disappearing completely at about 135 °C. The origin of this deep level is at present unknown.

TABLE II. Measured characteristic parameters of the annealed-in deep-level defects in n-silicon. $\sigma(\infty)$: thermal capture cross section for electron (n) or hole (p) obtained from the emission rate data. $N_T(T)$: typical annealed-in deep-level concentration; the annealing temperature after which N_T was measured is given in parentheses.

Peak name	Level position (eV)	$\sigma(\infty)$ ($\times 10^{-15}$) (cm^2)	$N_T(T)$ ($\times 10^{12}$) (cm^{-3})	T_{in} (°C)	T_{out} (°C)
E6	$E_c-0.315$	11.0(n)	4.0 (25 °C)	25	···
E7	$E_c-0.29$	1.10(n)	2.8 (244 °C)	150	~400
E8	$E_c-0.42$	0.27(n)	0.8 (227 °C)	227	>400
E9	$E_c-0.17$	0.84(n)	3.0 (288 °C)	244	>400
E10	$E_c-0.20$	0.26(n)	1.6 (400 °C)	340	>400
E11	$E_c-0.41$	10.2(n)	0.5 (340 °C)	227	>400
H3	$E_v+0.25$	66.2(p)	>4.8 (340 °C)	288	>400
H4			>2.5 (340 °C)	340	>400

B. E2 - electron level at $E_c-0.204$ eV

This is the dominant level observed in our α-irradiated samples. Its electron capture cross section and particularly the annealing behavior closely resemble those of the well-known oxygen-vacancy (O-V) complex, i.e., the A center commonly observed in irradiation studies on silicon. Although our activation energy appears to be significantly different than the usually cited value of 0.17 eV for the A level, it may be pointed out that there is a considerable range of values of the activation energy as well as the emission rates quoted in the literature for the A level. This dispersion in both these characteristics is generally attributed to the field-dependent thermal emission of electrons from the A center.[25] To that extent the deviation of our measured activation energy from the commonly quoted value is not a cause of major concern. We have tried to explicitly investigate the field dependence of the emission rate but could not find any measurable shift of the peak position of E2 with increasing bias. This apparent lack of field-dependence can, however, be understood in view of the fact that for our low-doped diodes the maximum electric fields that can be practically attained are too small to cause an observable increase of the emission rate.[26] Our somewhat higher observed activation energy would also be consistent with these low electric fields since one would expect the emission barrier energy to decrease with the increase of the field.

The production rate of the A level due to α irradiation is found to rise nonlinearly with the dose according to the approximate relationship $N_T \simeq 9\times 10^{-3}\,\phi^{1.45}$. It is interesting to note that both E1 and E2 show the same type of dose dependence (with different coefficients). This suggests that both these defects are probably the result of the same type of production mechanism which requires more than one alpha particle per defect center of the type E1 or E2.

C. E3 - electron level at $E_c-0.261$ eV

This level is the most easily identified level in our work. Its emission rate signature, activation energy, and annealing behavior all agree with those reported in the literature[27,28] for the doubly negatively charged acceptor level due to the divacancy complex $(V\text{-}V)^{--}$. Its production rate is found to be about 135 cm^{-1}.

D. E4 - electron level at $E_c-0.37$ eV

This level appearing as a shoulder of the peak due to the level E5 cannot be characterized accurately due to this strong overlap. This shoulder is seen to disappear at about 100 °C during our annealing work. This anneal out at relatively low temperatures is consistent with the fact that, as reported in our preliminary study,[20] this level is observed to anneal out during storage (~5 weeks) of the samples at room temperature. Walker and Sah[22] have reported a level at $E_c-0.358$ eV in the electron irradiation studies on Si

which is found to anneal out at temperatures ranging from 200 to 300 °C depending on the phosphorus doping level of their samples. Kimerling[23] and Brotherton and Bradley[4] have independently observed levels at similar positions in their electron- and γ-irradiation studies. In the case of Brotherton and Bradley, electron levels at $E_c-0.35$ eV and $E_c-0.36$ eV are observed only after annealing, their concentrations peaking at about 300 °C. The annealing behavior observed by Kimerling is also drastically different than for our level. It is, therefore, clear that our E4 level is distinctly different than these previously observed levels at similar position. Recently, however, Londos[24] has reported a level with activation energy 0.33 eV whose emission rate data seem to closely correspond with our data. No information regarding the annealing behavior of this level has, however, been given in this article.

E. E5 - electron level at $E_c-0.43$ eV

The two well-known candidates for this commonly observed level in irradiation studies on silicon are the singly charged acceptor state of the divacancy $(V\text{-}V)^-$ defect[27] and the E center,[4] i.e., the phosphorus-vacancy complex. These two deep-level defects are known to have similar activation energies and emission rate signatures and the DLTS peaks due to these generally overlap strongly. However, their anneal-out temperatures are in general, known to be widely different. While the E center anneals out at $\sim$150 °C–200 °C,[4,22,23] the $(V\text{-}V)^-$ defect tends to be stable up to about 300 °C or somewhat higher temperatures.[27]

It is thus clear from our annealing curves (Fig. 9) that the level E5 in our α-irradiated samples is created by the divacancy $(V\text{-}V)^-$ defect. We observe no step at $\sim$150 °C, indicating that no significant amount of the E center defect is produced in our samples. It is interesting to note that levels E3 and E5 always anneal out at the same temperature in all our samples. This confirms that E3 and E5 are indeed two different states of the same defect. Additional evidence for this conclusion is provided by the fact that these two levels have similar concentrations and concentration profiles (Fig. 5).

F. E6 - electron level at $E_c-0.315$ eV

This level appearing with a relatively low concentration in our irradiated samples shows interesting behavior. It is absent from our DLTS spectra taken soon after irradiation but appears within a few months of storage at room temperature. Thereafter it continues to grow slowly with time during long periods of storage (Fig. 8). A survey of the literature on radiation-induced defects in silicon shows no such effect although levels with similar activation energy and emission rates have been reported. For example, Hallên *et al.*[29] have observed a level at $E_c-0.31$ eV in their proton bombarded samples which seems to be very close to our E6 level, but they ascribe it to some hydrogen related defect, in agreement with the earlier work of Irmscher *et al.*,[30] since they do not observe it in their He^{2+} ion bombarded samples. Kimerling[23] has reported observing a level at $E_c-0.30$ eV in his 10 MeV electron irradiated samples but not in the samples exposed to 1.8 MeV α particles. His electron-induced level has a similar emission rate as our E6 level—however, Kimerling observes this level only after a heat treatment (anneal-in) at 150 °C and reports no buildup with room temperature storage similar to our case. We are, therefore, led to conclude that we are observing a new level whose generation is probably the result of a room temperature transformation of some radiation-induced secondary defect whose structure requires detailed investigation.

G. H1 - hole level at $E_v+0.352$ eV

This is one of the highest concentration defects produced by α irradiation in our samples. Its energy position and emission rate signature make it easy to identify this level with a commonly observed defect center in irradiation studies generally thought to be associated with a carbon related defect complex. The three candidates for this center discussed in the literature are the interstitial-substitutional carbon complex $(C_i\text{-}C_s)$,[31] the carbon-oxygen complex $(C_i\text{-}O_i)$[32,33] and the carbon-oxygen-vacancy complex (C-O-V).[34] Of these, the generally favored candidate for the deep level under discussion is the $C_i\text{-}O_i$ complex, although the question is not absolutely settled. This identification is particularly favored by the anneal-out behavior of this center. The $C_i\text{-}C_s$ center is argued to anneal out at about 300 °C, whereas the observed anneal-out temperature of the $E_v+0.352$ eV level in our study as well as in other works[22,34] is found to be 400 °C. The close tracking of this level and the level E2 identified with the A center during annealing (Fig. 9) may be an indication of the involvement of the interstitial oxygen in both defects.

H. H2 - hole level at $E_v+0.652$ eV

This is the deepest level observed in our work, although in the lowest concentration. In view of its position in the upper-half band gap of silicon, its observation in our minority-carrier (hole) emission DLTS spectrum is surprising. This obviously is a clear indication of its much larger capture cross section for holes as compared to that for electrons as can also be inferred from its $\sigma(\infty)$ value given in Table I. Comparison with literature shows that deep levels with such high activation energies have been rarely observed in irradiated silicon. The nearest in terms of activation energy are the two levels at $E_v+0.6$ eV and $E_v+0.68$ eV observed by Londos[35] in electron-irradiated p-type silicon. However, both these levels have been observed after a 90 min anneal at 470 K. Further, their emission rates are too low as compared to the level H2 observed by us. To the best of our knowledge, this is the first time such a level has been observed in irradiation studies on silicon.

I. Annealed-in levels

The deep levels arising during our isochronal thermal annealing treatment have been compared in detail with the levels observed by other workers during annealing of irradiated silicon. Two of our annealed-in levels, i.e., E8 at

$E_c-0.42$ eV and H3 at $E_v+0.25$ eV are very close to the $E_c-0.422$ eV level and $E_v+0.239$ eV level, respectively, observed by Walker and Sah[22] both with respect to their energy positions and detailed emission rate signatures.

The electron level E7 at $E_c-0.29$ V appears at about 150 °C and anneals out at about 400 °C. This annealing behavior is very similar to that of a level observed at $E_c-0.3$ eV by Kimerling[23] in his 1 MeV electron-irradiation studies, which he suggests to be associated with a divacancy-oxygen complex. Brotherton and Bradley[4] report a level at $E_c-0.35$ eV with similar annealing behavior in their 12 MeV electron-irradiated Schottky barrier samples, which is again associated with some divacancy complex. Recently Auret and Mooney[36] have also observed a level at $E_c-0.31$ eV with a somewhat higher anneal-in temperature of 200 °C. It is significant to note that our E7 level seems to arise concurrently with the decline in the concentration of the divacancy states E3 (V-V--/-) and E5 (V-V-/0) during annealing (Fig. 9). In view of this observation, it is very likely that this level is indeed a divacancy-related complex produced as a result of some transformation of the isolated divacancy defect during annealing.

The level E10 at $E_c-0.19$ V observed by us to anneal at $\sim$340 °C is probably the same level as observed by Auret and Mooney[36] to arise at $\sim$375 °C in their electron-irradiation work.

It is very interesting to compare the annealed-in defects with some of the deep levels revealed by our DLTS peak-shape analysis of the radiation-induced deep-level spectra presented in Sec. IV A. A comparison of the emission rate data of these two sets of levels reveals a close resemblance between the following levels: the E(0.17) level and the annealed-in level E9, the E(0.24) level and the annealed-in level E10 and the E(0.44) hidden level and the annealed-in level E8. This lends added support to the results of our peak-shape analysis insofar as this comparison confirms that indeed some of the levels hidden in our spectra of the as-irradiated samples are explicitly revealed as the dominant peaks are bleached out on high temperature annealing.

VI. CONCLUSIONS

Our study provides detailed information on the electrical characteristics of the deep-level defects introduced by 5.48 MeV α radiation in n-type silicon as summarized in Tables I and II. In addition, detailed data have been reported on the production rates and thermal annealing characteristics of these defeats. A thorough comparison with the available literature on radiation-induced defects leads us to the following interesting and new insights:

(a) Our production rates for the various deep levels due to α radiation are, in general, 10^3–10^4 times higher than those reported for electron irradiation of silicon.

(b) The disappearance of the level at $E_c-0.370$ eV (E4) and the slow emergence of a defect level at $E_c-0.315$ eV (E6) with storage time have never been reported before.

(c) An interesting but complex metastable structure has been observed close to the electron level (E2).

(d) The observation of a very deep level at $E_v+0.652$ eV (H2) with a very high hole capture cross section has been reported for the first time.

(e) A band of hole levels has been observed with the estimated top edge at about 0.35 eV above the valence band edge.

(f) A number of annealed-in levels have been observed some of which have not been reported before.

Whereas a lot of useful data have been provided by our study, clearly quite a few aspects of the observations listed above motivate further interesting investigations which would form the subject of our continuing work.

ACKNOWLEDGMENTS

We are grateful to Dr. Andrej Litwin of RIFA AB, Sweden for some of the samples. Thanks are also due to Dr. N. Baber for some useful discussions.

[1] D. S. Billington and J. H. Crawford Jr., *Radiation Damage in Solids* (Princeton University Press, Princeton, NJ, 1961).
[2] G. D. Watkins, J. R. Troxell, and A. P. Chatterjee, *Defects and Radiation Effects in Semiconductors,* edited by J. R. Albany (IOP, Bristol, 1979), 1978 Inst. Phys. Conf. Ser. No. 46, p. 16.
[3] See, for example, M. T. Asom, J. L. Benton, R. Sauer, and L. C. Kimerling, Appl. Phys. Lett. **51**, 256 (1987); E. Gürer, B. W. Benson, and G. D. Watkins, *Proceedings of the 16th International Conference on Defects in Semiconductors,* Pennsylvania, 1991 edited by G. Davies, G. Deleo, and M. Stavola (Trans. Tech., Zürich, 1992), p. 339.
[4] S. D. Brotherton and P. Bradley, J. Appl. Phys. **53**, 5720 (1982).
[5] K. Irmscher, H. Klose, and K. Maass, J. Phys. C: Solid State Phys. **17**, 6317 (1984).
[6] A. Chantre, M. Kechouane, and D. Bois, Proc. Mater. Res. Soc. Symp. **14**, 547 (1983).
[7] Y. Tokada, N. Shimizu, and A. Usami, Jpn. J. Appl. Phys. **18**, 309 (1979).
[8] L. C. Kimerling, IEEE. Trans. Nucl. Sci. **NS-23**, 1497 (1976).
[9] V. I. Gubskaya, V. I. Zvyagin, P. V. Kuchinskii, and V. M. Lomako, Sov. Phys. Semicond. **13**, 97 (1979).
[10] V. I. Gubskaya, P. V. Kuchinskii, V. M. Lomako, and A. P. Petrunin, Sov. Phys. Semicond. **15**, 243 (1979).
[11] L. S. Berman, A. P. Remenyuk, and V. B. Shuman, Sov. Phys. Semicond. **15**, 665 (1981).
[12] H. Indusekhar, V. Kumar, and D. Sengupta, Phys. Status. Solidi A **93**, 654 (1986).
[13] T. C. May and M. H. Woods, IEEE Trans. Electron. Devices **ED-26**, 2 (1979).
[14] T. Yoshihara, S. Takano, M. Kimato, and T. Nakano, IEEE Trans. Electron. Devices **ED-28**, 1198 (1981).
[15] D. V. Lang, J. Appl. Phys. **45**, 3023 (1974).
[16] G. Ferenczi and J. Kiss, Acta. Phys. Acad. Sci. Hungary **50**, 285 (1981).
[17] D. V. Lang, in *Thermally Stimulated Relaxation in Solids,* edited by P. Braunlich (Springer, New York, 1979), p. 93.
[18] E. Meijer, H. G. Grimmeiss, and L. Å. Ledebo, J. Appl. Phys. **55**, 4266 (1984).
[19] H. D. Barber, Solid State Electron. **10**, 1039 (1967).
[20] N. Zafar and M. Zafar Iqbal, J. Appl. Phys. **68**, 887 (1990).
[21] G. E. Jellison, Jr., J. Appl. Phys. **53**, 5715 (1982).
[22] J. W. Walker and C. T. Sah, Phys. Rev. B 7, 4587 (1973).
[23] L. C. Kimerling, *International Conference on Radiation Effects in Semiconductors,* Dubrovnik, 1976, edited by N. B. Urli and J. W. Corbett (IOP, Bristol, 1977), Inst. Phys. Conf. Ser. No. 31, p. 221.
[24] C. A. Londos, Phys. Status Solidi A **113**, 503 (1989).
[25] B. A. Komarov and V. I. Sopryakov, Phys. Status Solidi A **66**, 139 (1981), and references therein.
[26] K. Irmscher, H. Klose, and K. Maass, Phys. Status Solidi A **75**, K25 (1983).
[27] A. O. Evwaraye and E. Sun, J. Appl. Phys. **47**, 3776 (1976).
[28] F. P. Wang, H. H. Sun, and F. Lu, J. Appl. Phys. **68**, 1535 (1990).

[29] A. Hallên, B. U. R. Sundqvist, Z. Paska, B. G. Svensson, M. Rosling, and J. Tirên, J. Appl. Phys. **67**, 1266 (1990).
[30] K. Irmscher, H. Klose, and K. Maass, J. Phys. C **17**, 6317 (1984).
[31] K. L. Brower, Phys. Rev. B **9**, 2607 (1974).
[32] K. Thonke, G. D. Watkins, and R. Sauer, Solid State Commun. **51**, 127 (1984).
[33] G. Davies, E. C. Lightowlers, R. Wooley, R. C. Newman, and A. S. Oates, J. Phys. C **17**, L499 (1984).
[34] P. M. Mooney, L. J. Cheng, S. Süli, J. D. Gerson, and J. W. Corbett, Phys. Rev. B **15**, 3836 (1977).
[35] C. A. Londos, Phys. Status Solidi A **102**, 639 (1987).
[36] F. D. Auret and P. M. Mooney, J. Appl. Phys. **55**, 988 (1984).